Hotspot cooling with jumping-drop vapor chambers

Kris F. Wiedenheft,[1] H. Alex Guo,[1] Xiaopeng Qu,[1] Jonathan B. Boreyko,[1] Fangjie Liu,[1] Kungang Zhang,[1] Feras Eid,[2] Arnab Choudhury,[2] Zhihua Li,[2] and Chuan-Hua Chen[1,a)]
[1]*Department of Mechanical Engineering and Materials Science, Duke University, Durham, North Carolina 27708, USA*
[2]*Intel Corporation, Chandler, Arizona 85226, USA*

(Received 14 October 2016; accepted 17 February 2017; published online 3 April 2017)

Hotspot cooling is critical to the performance and reliability of electronic devices, but existing techniques are not very effective in managing mobile hotspots. We report a hotspot cooling technique based on a jumping-drop vapor chamber consisting of parallel plates of a superhydrophilic evaporator and a superhydrophobic condenser, where the working fluid is returned via the spontaneous out-of-plane jumping of condensate drops. While retaining the passive nature of traditional vapor-chamber heat spreaders (flat-plate heat pipes), the jumping-drop technique offers a mechanism to address mobile hotspots with a pathway toward effective thermal transport in the out-of-plane direction. *Published by AIP Publishing.* [http://dx.doi.org/10.1063/1.4979477]

Hotspots with high heat fluxes are prevalent in electronic systems with severe impacts on their performance and reliability.[1–3] Thermal management of hotspots is often complicated by their unsteady spatial distribution, e.g., in high-speed microprocessors with constantly changing computing tasks[4] and high-density power electronics with rapidly evolving output demands.[5] Mobile hotspots are inadequately addressed with existing hotspot cooling technologies. Among them, thermoelectric cooling can address hotspots reliably, but requires external power input and *a priori* knowledge of hotspot locations;[6,7] electrowetting can address mobile hotspots, but requires active power input with complex circuitry for digitized cooling;[8,9] convective cooling can handle large heat fluxes, particularly with phase change, but requires external pumping as well as knowledge of the hotspot location for optimized performances.[10,11] Unlike these technologies, flat-plate heat pipes (vapor chambers) offer completely passive cooling, which is enabled by the wicking return of the working fluid from the condenser to the evaporator.[12,13] Although vapor-chamber heat spreaders are known to exhibit a large effective thermal conductivity in plane, they suffer from poor thermal conductance in the out-of-plane direction because the wicking return only occurs within the wick structures lining the chamber walls.

In this Letter, we achieve hotspot cooling with a jumping-drop vapor chamber that employs an out-of-plane liquid return mechanism (Fig. 1). The jumping-drop chamber consists of parallel superhydrophilic and superhydrophobic plates that are sealed together with a vacuum gasket. The superhydrophilic plate is the evaporator with wick structures to distribute water, the working fluid. The superhydrophobic plate is the condenser that repels the condensing water drops and promotes their jumping return upon drop coalescence.[14–26] The coalescence-induced jumping is powered by surface energy and is perpendicular to the superhydrophobic condenser.[16,27] When a hotspot appears on the evaporator, the working fluid vaporizes around the hotspot and condenses on the opposing condenser. The growing condensate drops coalesce and jump away from the condenser, returning the working fluid back to the evaporator, right around the hotspot. The jumping-drop hotspot cooling technique in Fig. 1 offers a unique opportunity to passively address mobile hotspots while providing high out-of-plane conductance: (i) The passive cooling feature of conventional vapor chambers is retained by the self-propelled jumping drops, which are well below the capillary length and not affected by gravitational orientation. (ii) The high effective thermal conductivity in the out-of-plane direction results from the out-of-plane jumping return from the superhydrophobic condenser, assisted by the lateral wicking on the superhydrophilic evaporator. (iii) The management of mobile hotspots is enabled by the perpendicular jumping which directly returns the working fluid back to the hotspots as they appear.

Our hotspot cooling technique builds upon previous reports of jumping-drop vapor chambers.[28,29] To address

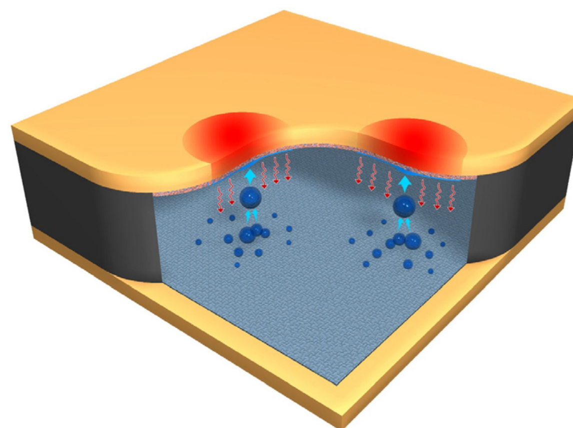

FIG. 1. Schematic of hotspot cooling with the jumping-drop vapor chamber. The top plate is the superhydrophilic evaporator covered with a water-filled wick. The bottom plate is the superhydrophobic condenser on which the condensate drops jump upon coalescence. The jumping mechanism returns the condensate drops to the evaporator, providing a mechanism to address mobile hotspots as they appear.

[a)]chuanhua.chen@duke.edu

localized hotspots with a much higher heat flux, two important modifications are introduced to the evaporator reported by Boreyko and Chen.[29] First, instead of a porous wick made of sintered copper particles, a micropillared wick is milled on the functional side of the copper evaporator (Alloy 101, 390 W/m·K) and rendered superhydrophilic by thermal oxidization. The squarely arranged pillars have a nominal cross-sectional area of 0.1 mm × 0.1 mm, a center-to-center separation of 0.2 mm, and a height of 1.0 mm. Empirically, the machined wick produced in this manner is compatible with the nanostructured superhydrophobic condenser described below, whereas the sintered wick in Ref. 29 typically leads to damage in the nanostructures and loss of superhydrophobicity at heat fluxes above 100 W/cm^2. Second, instead of a copper evaporator with a uniform thickness on the backside, a trench is formed by milling out the center region on the back (Fig. 2). Consequently, the center of the evaporator has a solid layer (excluding the wick structure) with a thickness of only 1.2 mm. This thickness is a compromise to provide sufficient structural rigidity while minimizing unintended heat spreading through the solid enclosure. Further experimental details can be found in Sec. S1 in the supplementary material.

The rest of our vapor chamber system essentially follows Ref. 29 with a few changes noted below. The superhydrophobic condenser is made of a copper substrate covered with silver nanoparticles by electroless galvanic deposition[30] and coated with a monolayer of 1-hexadecanethiol (VWR 200020-058). The vacuum seal between the evaporator and condenser is provided by mechanical compression using a Buna-N gasket (McMaster-Carr 8969K56-70A) with a compressed thickness of 1.8 mm. A small resistive heater (Am. Tech. Ceramics LR12010T0050JBK) with an area of $A = 2.5\,\text{mm} \times 5.1\,\text{mm}$ is soldered onto the back of the trenched evaporator to provide a localized heat load. After assembly by bolted compression, the recirculating fluid that runs through the condenser is set at 50 °C, and maintained at this temperature throughout the subsequent preparations and tests. The overall chamber is first brought to thermal equilibrium with the heater turned off. The chamber is evacuated with a vacuum pump (Edwards RV3) and then charged with 3.4 ml deionized water.[29] This charging volume is calculated to over-saturate the 1 mm-height wick structure. The extraneous working fluid is then removed with a brief exposure to the vacuum pump—the 1st secondary vacuum after charging. The system is allowed to thermally equilibrate prior to each round of secondary vacuum. The secondary vacuums remove noncondensable gases to improve the hotspot cooling performance, which is measured over a sweep of heat fluxes after a particular round of evacuation. The run-to-run variations of the vapor chamber performance are mainly due to the hand-controlled secondary vacuums. Empirically, four secondary vacuums produce consistent cooling performance, which may be further improved with additional vacuum pulls.

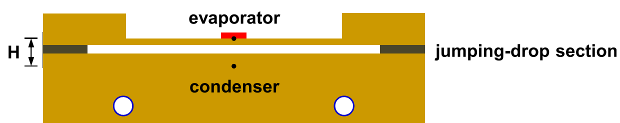

FIG. 2. The experimental setup with the cross-sectional view (to scale) cutting through the center plane of the chamber. The three-dimensional chamber geometry is detailed in Fig. S1 in the supplementary material. The jumping-drop section is enclosed by a 1.8 mm-thick gasket. The evaporator is locally heated, while the condenser is convectively cooled using the two embedded pipes. The temperature drop ΔT is measured across two probing locations (indicated by dots) with a separation H.

For thermal characterization, the temperature drop ΔT across the chamber is measured as a function of the hotspot heat flux q. At a particular heat flux, the temperature rise is recorded after the system is allowed to reach thermal equilibrium (for at least 5 min after a heat flux is imposed). A small thermocouple with a bead diameter of 75 μm (Omega Chal-003) is embedded underneath the resistive heater while the heater is soldered onto the evaporator. The heat flux q is nominally the input power divided by the cross-sectional area of the heater. Since the solder material is electrically conducting, the thermocouple measurement represents an *average* heater temperature.[31] The temperature of the condenser is probed with an embedded thermistor (Omega 44131). The vertical distance (H) between the centers of the two temperature probes, across which ΔT is measured, is 6.6 mm as depicted in Fig. 2.

Unlike previous reports with uniform heat fluxes, one-dimensional heat transfer can no longer be assumed in the present study focused on hotspot cooling. Consequently, many geometrical details are now important, and are accounted for by a numerical model (Comsol 4.2). In the model, the geometry of the solid enclosure is reproduced while excluding the thermistor hole in the condenser, the charging/evacuation ports, and the screw holes used for compression sealing. The overall chamber, including the jumping-drop section with a thickness given by the compressed gasket, is modeled as an isotropic solid material with a uniform effective thermal conductivity k_O; see Fig. S2 in the supplementary material. The heat produced by the resistive heater is modeled as a localized heat flux that is uniformly distributed across the heater area. The cooling pipes in the condenser assume a constant wall temperature, a reasonable assumption as described in Sec. S2 in the supplementary material. The rest of the chamber surface is assumed adiabatic. For a given set of boundary conditions, the numerical model is used to extract the difference between the area-averaged temperature underneath the heater and the pointwise temperature at the intended probing location in the condenser, in a manner mirroring the experimental measurements of ΔT as a function of q.

Using the numerical model, the $\Delta T(q)$ measurements of the hotspot cooling performance can be recast as effective thermal conductivities k_O for the overall chamber. If the heat flux is uniform across the evaporator, the effective thermal conductivity is simply $k_O = Hq/\Delta T$ assuming one-dimensional heat transport, as in Refs. 28 and 29. When the heat flux q is localized at a hotspot, the lateral heat spreading must be accounted for in addition to the vertical heat spreading (roughly across H) when extracting the effective conductivity. Consequently, a modified relationship is expected

$$k_O = \Gamma H q/\Delta T, \tag{1}$$

where the geometrical prefactor Γ accounts for the additional heat spreading in the lateral direction ($\Gamma < 1$). For the vapor

chamber in Fig. 2, which is simplified as an isotropic solid block in Fig. S2 in the supplementary material, the three-dimensional numerical model yields $\Gamma = 0.198$. For a thin heat spreader with an approximately uniform thickness H and a reasonably uniform temperature on the condenser side, Γ can be crudely approximated as[32]

$$\Gamma_{\mathrm{approx}} = 1 - e^{-\frac{8}{3\pi}\frac{a_e}{H}}, \tag{2}$$

where $a_e = \sqrt{A/\pi}$ is the effective radius of the heater of cross-sectional area A. For our chamber geometry, Eq. (2) yields $\Gamma_{\mathrm{approx}} = 0.228$ which is close to the exact value. The compact-form approximation in Eq. (2) is therefore useful for quick estimations of the heat spreading parameter Γ in lieu of exact but complex simulations.

The aforementioned experimental and numerical setups are employed to study the hotspot cooling performance of the jumping-drop chamber. In Fig. 3, the heat load is imposed by a single heater at the back center of the evaporator. After a particular round of secondary vacuum, the temperature drop across the chamber (ΔT) is measured against a sweep of hotspot heat fluxes (q) at 50 W/cm^2 increments. For each heat flux sweep, the vapor chamber is held horizontally with the superhydrophobic condenser either at the bottom or top, where the condensate drops jump either "against gravity" or "with gravity," respectively. The maximum heat flux tested is 400–450 W/cm^2, while the condenser is held at approximately 50 °C, so that the hotspot temperature does not exceed the thermal stability limit of the alkylthiol coating (approximately 70 °C). Below this maximum heat flux, dry-out is observed in the "5th secondary vacuum, against gravity" and "6th, with" data sets, as indicated by a quickly rising ΔT that has been similarly observed in the case of uniform heat fluxes. The experimental data in Fig. 3 can be transformed to the overall effective conductivities in Fig. 4 using Eq. (1) with the simulated value of $\Gamma = 0.198$.

We are now in a position to discuss the three advantages of the jumping-drop vapor chamber: self-propelled passive cooling, high out-of-plane conductance, and mobile hotspot

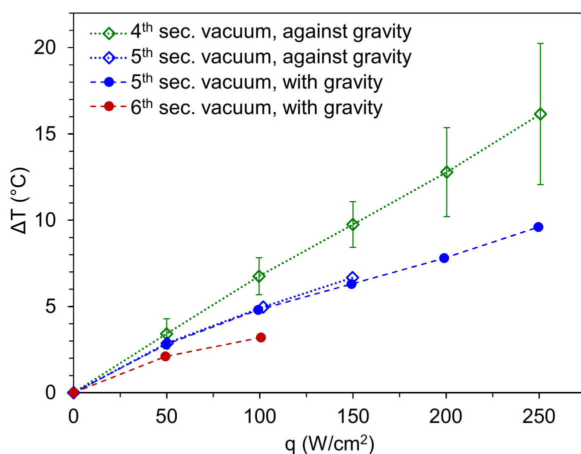

FIG. 3. The temperature drop ΔT across the vapor chamber as a function of the hotspot heat flux q. The direction of the jumping return is either "with gravity" or "against gravity." Each data set is taken after a particular round of secondary vacuum as indicated. The error bars on the "4th secondary vacuum, against gravity" case are the 95% confidence intervals based on three independent tests.

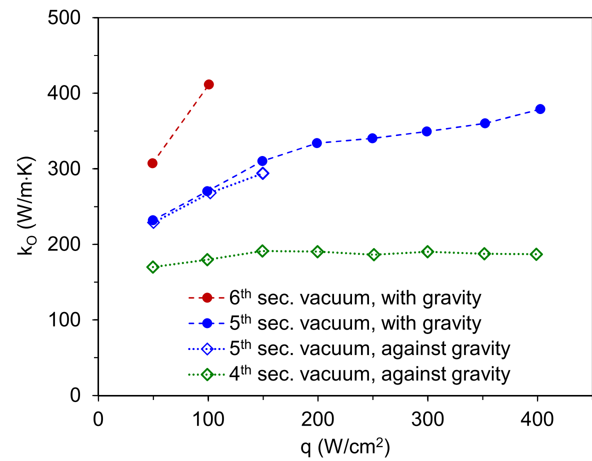

FIG. 4. The overall effective thermal conductivities are calculated from the measurements in Fig. 3 using Eq. (1) with the simulated value of $\Gamma = 0.198$. Only one of the "4th, against" data sets in Fig. 3 is used in Fig. 4. Some data at higher heat fluxes are not shown in Fig. 3, where the error bars are only assessed at heat fluxes up to 250 W/cm^2.

management. Our hotspot cooling technique is enabled by the self-propelled jumping return which is driven by intrinsic surface energy. As such, the jumping-drop technique offers passive cooling that neither requires active power input nor depends on external forces. Indeed, the jumping return has been shown to be independent of gravity as long as the gasket thickness is within 2 mm or so.[29] Our results in Fig. 3 with a gasket thickness of 1.8 mm confirm the orientation independence of the jumping return mechanism, where the "with" and "against" orientations following the 5th secondary vacuum yield essentially the same results at low heat fluxes. Since the jumping drops are too small for gravity to play a significant role in the liquid return mechanism, the delay of dry-out in the "with gravity" orientation is a reflection of the placement of the evaporator at the bottom, which facilitates the gravity-assisted escape of vapor bubbles during early-stage boiling.[12,28]

Our jumping-drop technique promises high effective conductance in the out-of-plane direction because it enables perpendicular liquid return for hotspot cooling. The overall effective conductivity k_O of the jumping-drop chamber in Fig. 4 is better than conventional vapor chambers which lack the perpendicular return mechanism. In a prior report by Sauciuc *et al.* that compares a conventional vapor chamber to solid spreaders, sufficient information is given (Fig. 9 of Ref. 33) to yield a calculated $k_O \approx 110$ W/m·K as defined in Eq. (1). In Fig. 4, we have achieved an overall effective conductivity that is close to 400 W/m·K, the thermal conductivity of copper. Since the chamber encasing is made of copper, the effective conductivity of the jumping-drop section must be comparable to 400 W/m·K too. The good performance of the jumping section is a result of the synergistic action of the perpendicular jumping return and the lateral wicking return. In our high-aspect-ratio vapor chamber, a significant portion of the vapor escaping from the hotspot is expected to condense into liquid drops nearby, i.e., around the condenser area directly opposite to the hotspot, while the rest of the vapor condenses farther away. The distributed condensation leads to both perpendicular thermal transport and lateral heat

spreading. The improvement in hotspot cooling performance with increasing rounds of secondary vacuums and higher heat fluxes is consistent with prior work based on uniform heat fluxes.[29] The secondary vacuums improve the condensation heat transfer by removing noncondensable gases. The vacuum pulls also remove some working fluid from the evaporator, likely leading to a receded meniscus in the wick and a reduced resistance of the wetted wick. As a side effect, repeated evacuations may remove too much working fluid, contributing to an eventual dry-out.

Our system is capable of managing mobile hotspots, toward which the working fluid is directly returned by the perpendicular jumping. In Fig. 5, two identical heaters are soldered onto the back of the evaporator, and a thermocouple is affixed to the evaporator beside each heater using a solder tape (JL Smith 131005), as depicted in the inset of Fig. 5(a). These heaters are separated by a 16 mm spacing and positioned symmetrically around the center of the evaporator. The experimental procedures are the same as before, except that the heat load is now provided by the two heaters which can be turned on separately or together. The heater configuration is denoted by q_1, q_2, and q_{12}, where the subscripts

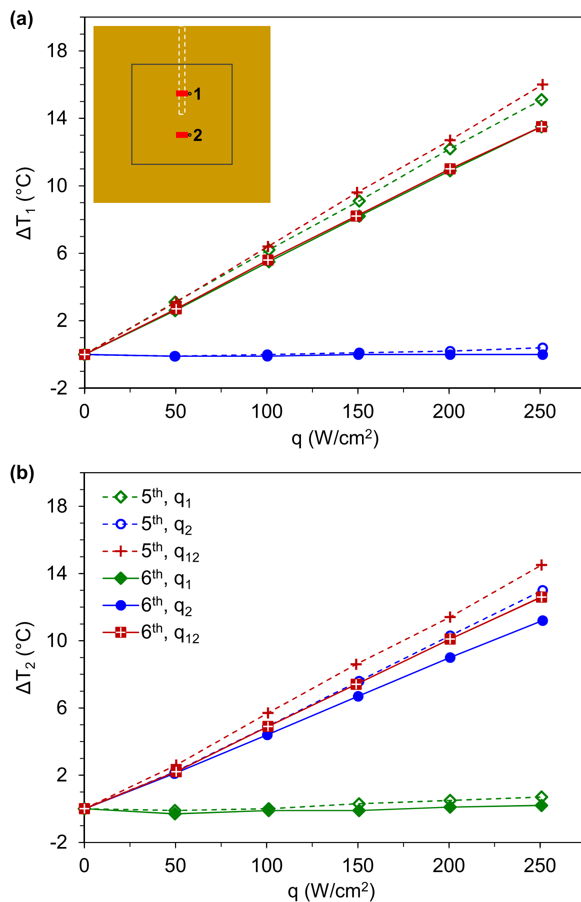

FIG. 5. Cooling of two hotspots that are individually controlled. The inset in (a) is a top view of the two-hotspot arrangement, with a thermocouple (black dot) affixed beside each heater. The condenser temperature is probed through a thermistor inserted into a hole (white dashed line) parallel to the superhydrophobic surface. The cooling pipes (not shown) are parallel to the thermistor hole. The subscripts in heat flux q indicate which heater is turned on, and the subscripts in the temperature rise ΔT indicate which thermocouple is used. The data sets are taken in the "with gravity" orientation after the 5th or 6th secondary vacuum.

indicate which heater is turned on. The same heat flux is imposed on each heater when both are on. The temperature rises with respect to the condenser temperature, ΔT_1 and ΔT_2, are measured at the respective heaters. As in the single-hotspot experiments, the cooling performance is enhanced with each round of secondary vacuums. Note that the evaporator has aged prior to the two-hotspot experiments, resulting in a somewhat degraded performance.

As a consequence of the perpendicular jumping return, distributed hotspots are addressed locally as they appear (Fig. 5). After the 6th secondary vacuum, there is no appreciable temperature rise measured at one location due to the other heater, so $\Delta T_1(q_2)$ and $\Delta T_2(q_1)$ are essentially zero. When heater 1 is on, its temperature rise is the same regardless of heater 2, i.e., $\Delta T_1(q_1)$ and $\Delta T_1(q_{12})$ are identical. This independence suggests that the heat load on heater 2 has not spread to the region around heater 1. The heat dissipation for heater 1 is complicated by the 2.6 mm-diameter thermistor hole, with its top surface approximately 2 mm beneath the condenser surface. Because of the reduced heat conduction on the condenser side opposing heater 1, the heat load imposed on this heater spreads farther away on the evaporator side. Consequently, $\Delta T_2(q_{12})$ is slightly larger than $\Delta T_2(q_2)$ to accommodate the small fraction of heat spread from heater 1.

In summary, we have demonstrated a hotspot cooling technique based on the jumping-drop vapor chamber, in which the self-propelled jumping motion of the condensate drops returns the working fluid from the superhydrophobic condenser back to the opposing superhydrophilic evaporator. The jumping-drop technique enables passive cooling without external power input, and facilities mobile hotspot management without prior knowledge of hotspot distribution. Compared to conventional vapor chambers without a perpendicular return mechanism, the jumping-drop system offers significantly enhanced thermal transport in the out-of-plane direction. In the context of hotspot cooling, we have demonstrated an overall effective thermal conductivity comparable to copper, but the hotspot cooling performance may be substantially improved. The wick in our system is relatively thick and may be significantly shortened to reduce its thermal resistance,[29] particularly if noncondensables are properly removed from the working fluid prior to charging (as in heat pipes[12]). The alkylthiol coating of the superhydrophobic condenser restricts its upper operating temperature, limiting the vapor temperature and the effectiveness of phase-change heat transfer. If an alternative coating is developed that is stable at higher temperatures yet immune to chemical cross-talks with the (oxide-coated) superhydrophilic evaporator, a better out-of-plane thermal conductance is expected in certain applications. One example is microelectronic cooling[1,34] where the working temperature can be significantly higher than 70° C, the approximate limit of thermal stability for the alkylthiol coating.

See supplementary material for details on experiments and modeling.

This work was supported by Intel Corporation and the National Science Foundation (CBET-12-36373). K.F.W. was

supported by the NSF Research Triangle MRSEC (DMR-11-21107) and the NSF Graduate Research Fellowship (DGF-11-06401). The Duke authors are grateful to Roger Chavez and Steve Kim (Duke) for their contributions to the experimental setup, and to Dr. Hao Yun (DuPont) for providing electroplating molds during the exploration of alternative wick structures. The authors also acknowledge Dr. Chia-Pin Chiu, Dr. Shankar Devasenathipathy, Dr. Chuan Hu, and Dr. Ravi Prasher (Intel) for helpful discussions.

[1] R. Mahajan, C.-P. Chiu, and G. Chrysler, Proc. IEEE **94**, 1476 (2006).
[2] A. Bar-Cohen and P. Wang, J. Heat Transfer **134**, 051017 (2012).
[3] C. Green, P. Kottke, X. Han, C. Woodrum, T. Sarvey, P. Asrar, X. Zhang, Y. Joshi, A. Fedorov, S. Sitaraman, and M. Bakir, J. Electron. Packag. **137**, 040802 (2015).
[4] H. F. Hamann, A. Weger, J. A. Lacey, Z. Hu, P. Bose, E. Cohen, and J. Wakil, IEEE J. Solid-State Circuits **42**, 56 (2007).
[5] M. Honsberg and T. Radke, Power Electron. Eur. **1**, 34 (2010), available at http://www.power-mag.com/pdf/feature_pdf/1269522044_Feature_Mitsubishi_Layout_1.pdf.
[6] B. Yang, P. Wang, and A. Bar-Cohen, IEEE Trans. Compon. Packag. Technol. **30**, 432 (2007).
[7] I. Chowdhury, R. Prasher, K. Lofgreen, G. Chrysler, S. Narasimhan, R. Mahajan, D. Koester, R. Alley, and R. Venkatasubramanian, Nat. Nanotechnol. **4**, 235 (2009).
[8] P. Y. Paik, V. K. Pamula, and K. Chakrabarty, IEEE Trans. VLSI Syst. **16**, 432 (2008).
[9] J.-T. Cheng and C.-L. Chen, Exp. Fluids **49**, 1349 (2010).
[10] S. Narayanan, A. G. Fedorov, and Y. K. Joshi, J. Micromech. Microeng. **20**, 075010 (2010).
[11] C. S. Sharma, G. Schlottig, T. Brunschwiler, M. K. Tiwari, B. Michel, and D. Poulikakos, Int. J. Heat Mass Transfer **88**, 684 (2015).
[12] A. Faghri, *Heat Pipe Science and Technology* (Taylor & Francis, 1995).
[13] J. A. Weibel and S. V. Garimella, Adv. Heat Transfer **45**, 209 (2013).
[14] M. Kollera and U. Grigull, Heat Mass Transfer **2**, 31 (1969).
[15] C. H. Chen, Q. Cai, C. Tsai, C. L. Chen, G. Xiong, Y. Yu, and Z. Ren, Appl. Phys. Lett. **90**, 173108 (2007).
[16] J. B. Boreyko and C.-H. Chen, Phys. Rev. Lett. **103**, 184501 (2009).
[17] C. Dietz, K. Rykaczewski, A. Fedorov, and Y. Joshi, Appl. Phys. Lett. **97**, 033104 (2010).
[18] X. Chen, J. Wu, R. Ma, M. Hua, N. Koratkar, S. Yao, and Z. Wang, Adv. Funct. Mater. **21**, 4617 (2011).
[19] M. He, X. Zhou, X. Zeng, D. Cui, Q. Zhang, J. Chen, H. Li, J. Wang, Z. Cao, Y. Song, and L. Jiang, Soft Matter **8**, 6680 (2012).
[20] N. Miljkovic, R. Enright, Y. Nam, K. Lopez, N. Dou, J. Sack, and E. N. Wang, Nano Lett. **13**, 179 (2013).
[21] K. Rykaczewski, A. T. Paxson, S. Anand, X. Chen, Z. Wang, and K. K. Varanasi, Langmuir **29**, 881 (2013).
[22] N. Miljkovic, D. J. Preston, R. Enright, and E. N. Wang, Appl. Phys. Lett. **105**, 013111 (2014).
[23] J. Tian, J. Zhu, H.-Y. Guo, J. Li, X.-Q. Feng, and X. Gao, J. Phys. Chem. Lett. **5**, 2084 (2014).
[24] X. Chen, J. A. Weibel, and S. V. Garimella, Adv. Mater. Interfaces **2**, 1400480 (2015).
[25] S. Q. Cai and A. Bhunia, J. Heat Transfer **139**, 041501 (2017).
[26] R. Enright, N. Miljkovic, J. L. Alvarado, K. Kim, and J. W. Rose, Nanoscale Microscale Thermophys. Eng. **18**, 223 (2014).
[27] F. Liu, G. Ghigliotti, J. J. Feng, and C. H. Chen, J. Fluid Mech. **752**, 39 (2014).
[28] J. B. Boreyko, Y. Zhao, and C.-H. Chen, Appl. Phys. Lett. **99**, 234105 (2011).
[29] J. B. Boreyko and C.-H. Chen, Int. J. Heat Mass Transfer **61**, 409 (2013).
[30] I. A. Larmour, S. E. Bell, and G. C. Saunders, Angew. Chem. **119**, 1740 (2007).
[31] J. Nicholas and D. R. White, *Traceable Temperatures: An Introduction to Temperature Measurement and Calibration* (Wiley, 2002).
[32] H. A. Guo, K. F. Wiedenheft, and C.-H. Chen, "Hotspot size effect on conductive heat spreading," IEEE Trans. Compon. Packag. Manuf. Technol. (submitted).
[33] I. Sauciuc, G. Chrysler, R. Mahajan, and R. Prasher, IEEE Trans. Compon. Packag. Technol. **25**, 621 (2002).
[34] A. Majumdar, Nat. Nanotechnol. **4**, 214 (2009).